ELSEVIER

Physica A 316 (2002) 233–249

PHYSICA A

www.elsevier.com/locate/physa

Multiscality in the dynamics of coupled chaotic systems

A.N. Pavlov[a,*], O.V. Sosnovtseva[a,b], A.R. Ziganshin[a], N.-H. Holstein-Rathlou[c], E. Mosekilde[b]

[a] *Nonlinear Dynamics Laboratory, Department of Physics, Saratov State University, Astrakhanskaya St. 83, 410026 Saratov, Russia*

[b] *Department of Physics, Technical University of Denmark, 2800 Kgs. Lyngby, Denmark*

[c] *Department of Medical Physiology, Panum Institute, University of Copenhagen, 2200 Copenhagen N, Denmark*

Received 20 May 2002

Abstract

We investigate the scaling features of complex motions in systems of two coupled chaotic oscillators by means of the wavelet-transform modulus maxima method and the detrended fluctuation analysis. We show that the transition from asynchronous to synchronous dynamics typically reduces the degree of multiscality in the characteristic temporal scales. Correlation properties caused by adjustment of the involved time scales are discussed, and experimental results for coupled functional units of the kidney are analyzed.

PACS: 05.40.+j; 05.45.Tp; 02.50.Ey

Keywords: Scaling; Multifractality; Phase synchronization; Wavelet transform

1. Introduction

Synchronization is a universal phenomenon in the interaction of nonlinear oscillators [1,2]. Within the frameworks of the classical theory, synchronization involves the entrainment of periodic processes and a locking of their frequencies to rational ratios. Synchronization may also take place via the suppression of the inherent dynamics of one of the interacting oscillators. Coupled chaotic oscillators demonstrate a significantly

* Corresponding author. Fax: +7-8452-514549.
E-mail address: pavlov@chaos.ssu.runnet.ru (A.N. Pavlov).

0378-4371/02/$ - see front matter
PII: S0378-4371(02)01202-5

wider range of entrainment forms, depending on the degree to which the interacting units can adjust their motions relative to one another. Examples of such chaotic entrainment phenomena are full synchronization [3,4], lag synchronization [5], generalized synchronization [6], and phase synchronization [7]. The phenomenon of chaotic synchronization finds a variety of technical applications in secure communication and in the surveillance and control of systems that display complex dynamics [3,8]. At the same time, synchronization of chaotic oscillators may play an essential role in the dynamics of many biological systems such as, for instance, the nephrons of the kidney and the insulin producing beta-cells of the pancreas [9].

During the last few years the interactive dynamics of chaotic systems has been the topic of a large number of studies, and different criteria to diagnose the synchronous state have been proposed. For oscillators that demonstrate the period-doubling route to chaos such diagnostics can often be provided by means of Fourier power spectra [10]. The spectral analysis allows us to search regions in parameter space where a locking of the basic frequencies takes place (similar to the Arnol'd tongues of coupled limit cycle oscillators). Another technique operates with the mutual instantaneous phases of the oscillators and defines entrainment as the appearance of some restricted variation between them [7]. This allows us to diagnose a state of chaotic phase synchronization where the oscillators adjust their phases respective to one another, but the amplitudes vary quite differently. Among the useful tools to study chaotic synchronization phenomena are also the coherence function or cross-spectrum [10], the mean return time to a Poincaré section [11], the transverse Lyapunov exponents [2], the diffusion coefficient of the phase difference [12], etc.

Interaction of chaotic oscillators changes the structure of the attractors that exist in the absence of coupling. These changes are reflected in the characteristic temporal scales and, hence, in the return times to a Poincaré section. Sequences of return times corresponding to chaotic motions have complex multiscale structures and can sometimes be considered as examples of the so-called multifractal processes [13–15]. Unlike homogeneous signals with a well-defined monoscale structure, such as $1/f$, white, or Brownian noise, the local scaling for multifractals does not remain the same throughout the evolutionary dynamics [15,16].

In practice, the scaling features of complex processes can be studied by means of various numerical approaches originating in classical correlation and Fourier analyses. The shapes of the correlation function $C(\tau)$ and the spectral density $S(f)$ allow one to conclude whether the scaling behavior of a time series can be described by power-law dependences of the type $C(\tau) \sim \tau^{-\rho}$ and $S(f) \sim f^{-\nu}$ with the single exponents ρ or ν. One of the disadvantages of these two approaches arises from their restriction to stationary data. Since many processes in Nature are highly inhomogeneous and nonstationary, from the viewpoint of possible applications the attractiveness of a particular technique depends on its generality (e.g., its lack of restrictions with respect to the homogeneity and the stationarity of the data series). Among such rather universal (and at the same time effective) tools for signal processing the detrended fluctuation analysis (DFA) [17] and the wavelet transform modulus maxima (WTMM) method [18,19] are particularly useful. The DFA-technique represents a variant of the root mean-square analysis of a random walk allowing us to investigate scaling properties of

nonstationary time series and clearly detect the presence of long-range correlations. Within this framework, the standard error of a linear interpolation of a random walk versus the size of the interpolation segment is analyzed. The WTMM-approach is related to the methods for studying multifractal phenomena and addresses the description of complex signals by using the notion of the *singularity spectrum* $D(h)$, where D is the fractal dimension of the subset of data characterized by the so-called Hölder exponent h [18,19]. The values of the Hölder exponents quantify the local scaling and, in general, do not coincide for different parts of an inhomogeneous process.

In the present paper, we investigate the transitions from an asynchronous to a synchronous regime for systems of two coupled chaotic oscillators in terms of the multiscality in their motions. Using both the DFA- and the WTMM-approaches, we study the structure of return time sequences for various processes in the complex dynamics of the interacting units. We start with a system of coupled Rössler oscillators that serve as a simple model demonstrating the period-doubling route to chaos. Each subsystem in this model has a clearly expressed basic frequency. Next, we extend our approach to systems with several characteristic time scales, being deterministic or statistical in origin. We consider two coupled Lorenz systems and a model of interacting nephrons in the kidney [9]. Chaotic motion in the Lorenz oscillator can be quantified by means of two frequencies: the first is associated with the movement around one of the unstable foci, and the second corresponds to the switching process when the unit is considered as a bistable system [20]. The nephron model [21] represents an example of a system that displays oscillations at two different characteristic scales, namely relatively fast oscillations associated with the myogenic dynamics of the afferent arterioles, and slower oscillations arising from the delay in the tubuloglomerular control of the incoming blood flow. The two time scales can be studied separately by taking different phase variables (or secant planes). We show that the interaction of coupled chaotic systems significantly changes the scaling properties of return time series leading to the loss of multiscality (or more generally to a reduction of its degree). We discuss correlation changes at the transition to the synchronous state and report features of multifractal characterization of the phase synchronization phenomenon for the considered models. Finally, experimental results for nephrons displaying complex oscillations in their tubular pressures are analyzed, both for the case when the nephrons are synchronized and for the case of nonsynchronized dynamics.

2. Methods

2.1. Detrended fluctuation analysis

The DFA-approach is based on the idea of construction a running sum from a data series $z(i)$, $i=1,\ldots,N$; over a given time scale. Such a procedure implies the building of a random walk with the values of the original data $z(i)$ used as increments.

An algorithm for detrended fluctuation analysis has several stages [17]. First, the mean value $\bar{z}$ is removed from $z(i)$ and the running sum is constructed as follows: $y(k)=\sum_{i=1}^{k}[z(i)-\bar{z}]$. Second, $y(k)$ is divided into nonoverlapping boxes of length

n, and in each box the line segment representing the *local trend* $y_n(k)$ is estimated via a least-squares fitting. The difference between the original walk displacement $y(k)$ and the local trend $y_n(k)$ is considered as the *detrended walk* [22]. After subtracting $y_n(k)$ from $y(k)$ the root mean-square fluctuation $F(n)$ is estimated:

$$F(n) = \sqrt{\frac{1}{N}\sum_{k=1}^{N}[y(k) - y_n(k)]^2}\,. \tag{1}$$

Such calculations are performed for a wide range of values of the box length. Further, one searches for a power law describing the dependence of the fluctuation on the box size: $F(n) \sim n^{\alpha}$, i.e., for a linear relationship between $\lg F$ and $\lg n$ that signals the presence of scaling. In practice the exponent α, being the slope of the corresponding line, may not be constant for different regions of n. This reflects a varying scaling behavior of the data series, and in such situations more detailed analysis based on estimation of local exponents can be performed [23].

Numerical values of α characterize different types of correlations if $\alpha \neq 0.5$ and uncorrelated dynamics for $\alpha = 0.5$. In particular, $0.5 < \alpha < 1$ is related to power-law correlations where large values in the series of data are more probably to appear after large values, and vice versa. The range $0 < \alpha < 0.5$ reflects anti-correlated behavior (alternation between small and large values). $\alpha > 1$ marks correlations that are not of a power-law form, and $\alpha = 1$ corresponds to $1/f$-noise [17].

2.2. WTMM-technique

Another approach to the study of complex scaling phenomena consists in the use of the concept of multifractals [13,14]. Initially, this concept was introduced for singular measures and provided a statistical description of their scaling properties in terms of the so-called singularity spectrum [14].

However, from the application point of view the possibility to analyze singular functions (signals) is more attractive. Several attempts have been made to extend the idea of multifractals to this situation. A first attempt was the structure function method originally proposed to investigate fully developed turbulent flows [24]. Later, the wavelet based multifractal formalism (the WTMM-approach) has appeared [18,19] and it is now the more popular technique for studying multiscale phenomena in nonstationary and inhomogeneous processes.

The analysis of a function $f(x)$ with the WTMM-approach is performed in the following way. In the first stage, the wavelet transform coefficients are estimated:

$$T_{\psi}[f](x_0, a) = \frac{1}{a}\int_{-\infty}^{\infty} f(x)\psi\left(\frac{x - x_0}{a}\right)\mathrm{d}x\,. \tag{2}$$

Often, a random walk displacement is considered for $f(x)$. a is the scale parameter, and ψ is the wavelet "mother" function that can have a rather arbitrary shape, although it should be soliton-like with zero average. In this work, we used the so-called *Mexican*

hat wavelet which is the second derivative of a Gaussian function:

$$\psi = \frac{\mathrm{d}^2}{\mathrm{d}x^2}\left[\exp\left(-\frac{x^2}{2}\right)\right] . \tag{3}$$

A local singular behavior of $f(x)$ at the point x_0 results in an increase of $|T_\psi[f](x,a)|$ as $x \to x_0$ and can be characterized by the Hölder exponent $h(x_0)$ that quantifies the scaling of the wavelet coefficients for small a: $T_\psi[f](x_0,a) \sim a^{h(x_0)}$.

Further, the statistical description of local singularities is performed using the notions of the *singularity spectrum* $D(h)$ and of the *partition function* $Z(q,a)$ [19]. Briefly speaking, $Z(q,a)$ is the sum of qth powers of the local maxima of $|T_\psi[f](x,a)|$ at the scale a [28]. It is expected that for small values of a the partition function follows the power law [18,19]:

$$Z(q,a) \sim a^{\tau(q)} \tag{4}$$

with the scaling exponents $\tau(q)$. The variation with powers of q allows us to obtain a linear dependence $\tau(q)$ with the single Hölder exponent $h(q) = \mathrm{d}\tau(q)/\mathrm{d}q = const$ in the case of monofractal objects and a nonlinear function with a large number of exponents $h(q)$ for multifractals. Finally, the singularity spectrum $D(h)$ is estimated by means of the Legendre transform: $D(h) = qh(q) - \tau(q)$.

The partition function $Z(q,a)$ reflects the scaling of large fluctuations in data series (strong singularities) for positive q and the scaling of small fluctuations (weak singularities) for negative q. In analogy with the DFA-technique, the values of the Hölder exponents allow us to make conclusions about the presence of anti-correlated dynamics ($0 < h < 0.5$), correlated behavior ($h > 0.5$), or about the absence of correlations ($h = 0.5$) [15].

3. Scaling features of return time sequences

3.1. Coupled Rössler oscillators

Let us start with a system of two coupled Rössler oscillators [7]:

$$\begin{aligned}
\frac{\mathrm{d}x_{1,2}}{\mathrm{d}t} &= -\omega_{1,2}y_{1,2} - z_{1,2} + \gamma(x_{2,1} - x_{1,2}) , \\
\frac{\mathrm{d}y_{1,2}}{\mathrm{d}t} &= \omega_{1,2}x_{1,2} + Ay_{1,2} , \\
\frac{\mathrm{d}z_{1,2}}{\mathrm{d}t} &= B + z_{1,2}(x_{1,2} - \mu) ,
\end{aligned} \tag{5}$$

where the parameters A, B, and μ govern the dynamics of each subsystem, and γ is the coupling parameter. $\omega_1 = \omega_0 + \delta$ and $\omega_2 = \omega_0 - \delta$ are the basic frequencies of the two oscillators and δ is the mismatch between them. In our study $A = 0.15$, $B = 0.2$, $\gamma = 0.02$, $\mu = 6.8$, and $\omega_0 = 1.0$. System (5) demonstrates a variety of coexisting synchronous regimes as well as different types of asynchronous dynamics. A detailed analysis of this model was performed by Postnov et al. [25]. Using partly the designations of

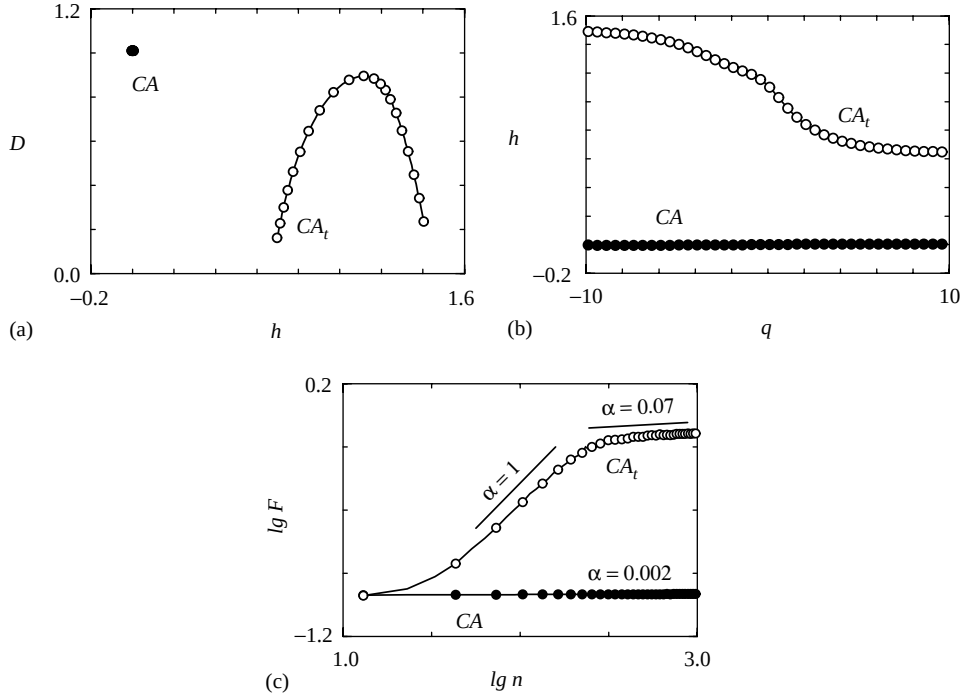

Fig. 1. Scaling properties of the synchronous chaotic attractor CA (black circles) and the asynchronous attractor CA_t (white circles): (a,b) singularity spectra $D(h)$ and Hölder exponents $h(q)$ obtained by the WTMM-approach; (c) root mean square fluctuations $F(n)$ (in double logarithmic plot) of the DFA-technique.

that work, we label the synchronous chaotic attractors as CA, and the asynchronous chaotic regime (torus-chaos) as CA_t. Strictly speaking, a set of chaotic solutions with different phase shifts exist inside the synchronization region. That is why it will be more correctly to associate some index with CA showing to which attractor family it relates. However, regimes of phase multistability have rather similar scaling properties [26]. Hence, this aspect is not of major importance for the present study.

The transition through the boundary of the synchronization region (from CA to CA_t) taking place with increasing mismatch parameter δ changes the structure of times when the phase space trajectory returns to a Poincaré section. To show this let us choose the secant plane $x_2 = 0$ and consider the shapes of singularity spectra $D(h)$ calculated from return time sequences for the two attractors (Fig. 1a). We clearly see that the width of $D(h)$ for the asynchronous regime CA_t is significantly larger than for CA (where $D(h)$ is represented by a single point). This means that the phase synchronization of the oscillations for the considered system involves a loss of multiscality in the return time dynamics: A complex structure of the return time sequence for the asynchronous attractor requires a large number of Hölder exponents to characterize its scaling properties fully (Fig. 1b, white circles). However, the dynamics of return times

for the synchronous chaotic motion is characterized by a nearly constant value of $h(q)$ (Fig. 1b, black circles at $h(q) \approx 0$).

As shown in our previous paper [26], the width of the singularity spectrum for different synchronous regimes can vary. Return time sequence can usually not be described as a monofractal object with $D(h)$ consisting of nearly a single point. Moreover, estimation of the Hölder exponents for large numerical values of q is typically sensitive to computational parameters like the range used for fitting $\tau(q)$. That is why we shall speak about the degree of multifractality (multiscality) rather than making conclusions as to whether an object under study displays a mono- or a multifractal structure. By performing an analysis of the scaling properties for various regimes in the interacting Rössler systems we have found that this degree is significantly smaller for all types of synchronous oscillations than for the complex motions outside the synchronization region.

Another distinction between the singularity spectra shown in Fig. 1a consists in the increase of the Hölder exponents $h(q)$ for the asynchronous dynamics. This indicates a change of correlation. Such a variation can be quantified by the difference in the numerical values of the exponents h for $q = 0$ related to the maxima of $D(h)$-spectra. Because the fractal dimensions D are both close to 1 for the chosen regimes if $q=0$, we need to know only the Hölder exponents $h(q)$ to characterize the location of singularity spectrum as well as the degree of multiscality. Hence, for the aims of our work it is enough to consider the dependence $h(q)$ without the shape of $D(h)$.

Correlation properties of return time sequences can also be analyzed within the framework of the DFA-technique. In the synchronous regime (attractor CA) the dependence $\lg F$ *vs.* $\lg n$ is described by a single scaling exponent $\alpha \approx 2 \times 10^{-3}$ (Fig. 1c, black circles). This value of α corresponds to strong anti-correlations in the return time dynamics: the probability of alternation between large and small (compared to the average) return times is close to 1 (this situation is typical for weak chaos developed via a period-doubling cascade). However, the asynchronous motion (CA_t) cannot be characterized by a single quantity. In an interval around $\lg n = 2.0$ the local exponent takes on a value near 1.0 (correlated behavior, the case of $1/f$-noise), i.e., we observe a smooth sequence of return times unlike the dynamics of the synchronous regime. In both regions of short- and long-range correlations (small and large n, respectively) the local scaling exponents decrease. By analogy with the width of the singularity spectrum for the WTMM-method let us introduce a measure of multiscality for the DFA-approach. Below we shall denote the range of Hölder exponents (the width of the $D(h)$-spectrum) as Δ_h, and the range of scaling exponents of the DFA-technique as Δ_α, the last quantity being the difference between the maximal and the minimal local values of α.

Fig. 2 clearly shows how the transition to asynchronous dynamics is diagnosed by both approaches. For the coupled Rössler oscillators this transition is accompanied by a significant increase of the multiscality measures (Δ_h, Δ_α - Figs. 2a and b) and by changes of the correlation type ($\bar{\alpha} < 0.5$ in the synchronous case whereas $\bar{\alpha} > 0.5$ for the asynchronous motions—Fig. 2a). Abrupt changes in the considered characteristics under variation of the control parameter δ mark the boundary of the synchronization region. Rather similar results are obtained for other secant planes ($x_1 = 0$, $y_1 = 0$,

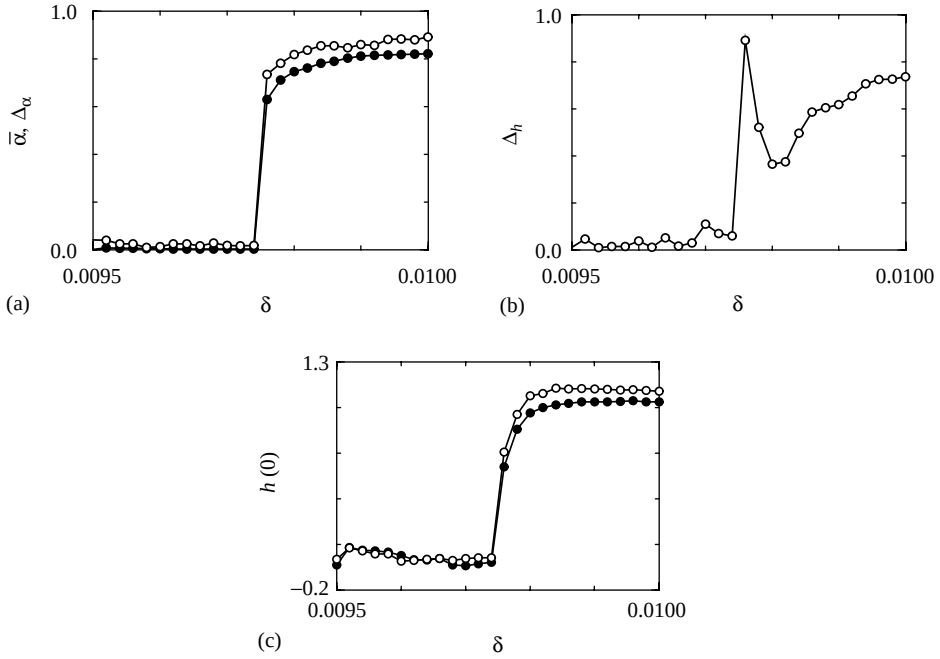

Fig. 2. Scaling characteristics of the transition from the synchronous to the asynchronous dynamics that takes place at $\delta \approx 0.00975$: (a) mean values of scaling exponents of the DFA-technique (black circles) and the scaling range Δ_α (white circles) as functions of the mismatch parameter; (b) the measure of multiscality Δ_h; (c) Hölder exponents corresponding to maxima of the singularity spectra estimated from sequences of return times to the secant planes $x_1 = 0$ (black circles) and $x_2 = 0$ (white circles).

$y_2 = 0$, etc.), i.e., particular regimes of both subsystems are quantified by similar scaling characteristics. Note also, that the chaotic phase synchronization in Eq. (5) removes differences between the complex motions of the interacting units: Scaling properties become closer inside the synchronization region (Fig. 2c).

3.2. Coupled Lorenz systems

The dynamics of each Rössler oscillator is characterized by a single temporal scale (the basic period of oscillations or the basic frequency). Let us now discuss a more complicated case in which the motion of the individual unit displays several different time scales. As the first example we have chosen the model of coupled Lorenz systems [27]:

$$\frac{\mathrm{d}x_{1,2}}{\mathrm{d}t} = \sigma(y_{1,2} - x_{1,2}) + \gamma(x_{2,1} - x_{1,2}) ,$$

$$\frac{\mathrm{d}y_{1,2}}{\mathrm{d}t} = r_{1,2}x_{1,2} - x_{1,2}z_{1,2} - y_{1,2} ,$$

$$\frac{\mathrm{d}z_{1,2}}{\mathrm{d}t} = x_{1,2}y_{1,2} - z_{1,2}b , \qquad (6)$$

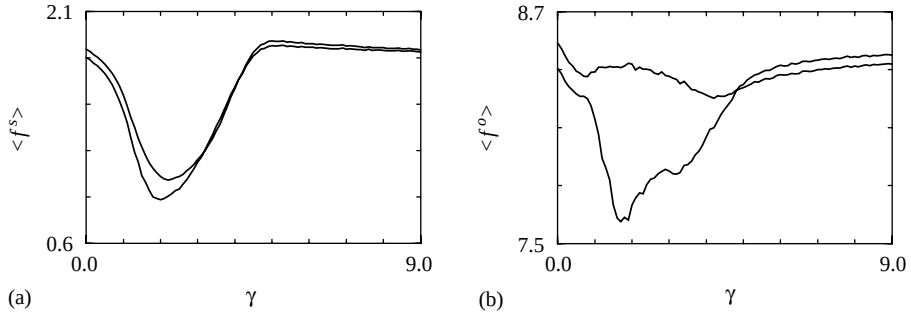

Fig. 3. Mean frequencies of switchings $\langle f^s \rangle$ and mean frequencies of oscillations $\langle f^o \rangle$ for the two interacting subsystems as functions of the coupling parameter γ. Note the initial reduction of the switching frequencies and the initial desynchronization of the two oscillators as the coupling parameter is increased.

where $\sigma = 10$, $r_1 = 28.8$, $r_2 = 28$, and $b = 8/3$. Each unit of Eq. (6) may be considered as a bistable system [20] that demonstrates switchings between the states "+1" and "−1" introduced as follows:

$$\hat{x}_{1,2} = \begin{cases} +1, & x_{1,2} > 0\,, \\ -1, & x_{1,2} < 0\,. \end{cases} \tag{7}$$

The mean switching period $\langle T^s \rangle$ (or the mean frequency $\langle f^s \rangle = 2\pi/\langle T^s \rangle$) is one of the statistical time scales that describe the dynamics of each subsystem. Another statistical time scale is related to rotations of the phase space trajectory around one of the unstable focus points. The corresponding mean frequency of rotations (or oscillations) is denoted as $\langle f^o \rangle$. Fig. 3 shows the behavior of these frequencies versus the coupling parameter γ. According to this figure, model (6) demonstrates a growing of difference between the frequencies $\langle f^s \rangle$ and $\langle f^o \rangle$ of the two subsystems with increasing γ up to the value $\gamma \approx 2.0$, i.e., an initial desynchronization effect is observed. This feature of the coupled Lorenz systems was reported by Anishchenko et al. [27]. With further increase of γ, first a synchronization of switchings and then a synchronization of oscillations take place.

Let us see how the different entrainment forms are reflected in the structure of the return time series (here we use the secant planes $z_1 = 30$ and $z_2 = 30$). As one can see in Fig. 4a, the scaling exponents of the DFA-approach decrease in the synchronization region ($\gamma > 6$). This means that with increasing γ the probability of alternation between large and small values of the return times (anti-correlations) increases. We suppose that the complex shape of the dependence $\bar{\alpha}(\gamma)$ with "plateaus" in the regions around $\gamma \approx 3$–4 and $\gamma > 6$ may be connected with the existence of the two time scales. Fig. 4a also shows how the scaling properties of the synchronous oscillations become closer for the two subsystems with strong coupling ($\gamma > 6$). Moreover, the scaling properties are close to the results for noninteracting dynamics ($\gamma = 0$). In this way, the wavelet-based technique testifies to the complex dependence of the scaling characteristics as functions of the coupling strength (Fig. 4b), and it demonstrates the decreasing degree of multiscality (Δ_h) for strong interaction.

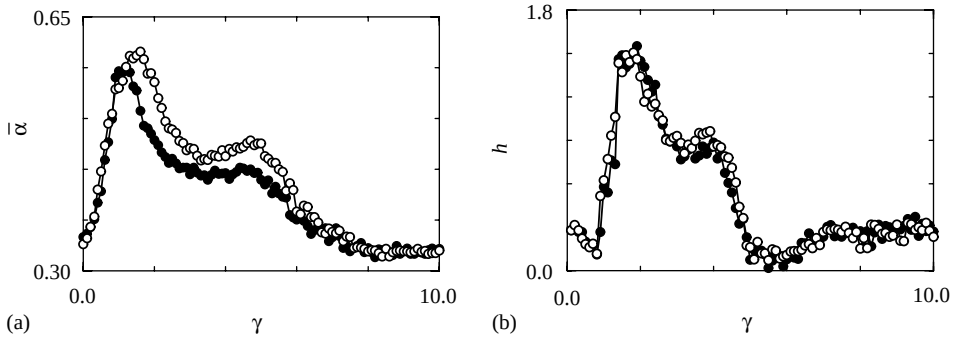

Fig. 4. Scaling exponents of the DFA-approach $\bar{\alpha}$ and measures of multiscality Δ_h estimated from return times to the Poincaré sections $z_1 = 30$ (white circles) and $z_2 = 30$ (black circles), respectively. Note the reduction of multiscality in the synchronization regime $\gamma > 6$.

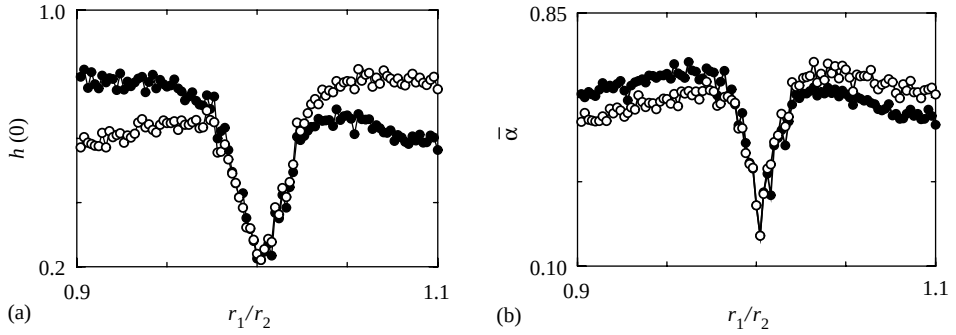

Fig. 5. Hölder exponents corresponding to maxima of singularity spectra and scaling exponents of the DFA-approach estimated from sequences of return times to the secant planes $z_1 = 30$ (black circles) and $z_2 = 30$ (white circles) vs. the ratio r_1/r_2 ($\gamma = 4.5$).

Besides the coupling parameter we can vary the mismatch between r_1 and r_2 in Eqs. (6). According to the WTMM-approach, the locations of the singularity spectra do not coincide for interacting subsystems outside the synchronization region, unlike the case of synchronous motions (Fig. 5a). Again we see that phase synchronization brings the scaling properties of the individual oscillators closer to one another. Here, the values $h(0)$ change rather smoothly with increasing mismatch. The minimum of the variation of $h(0)$ with r_1/r_2 corresponds to the identical case ($r_1/r_2 = 1$), characterized by the strongest anti-correlations (Fig. 5b) in comparison with other values of r_1/r_2.

Obviously, by analogy with the coupled Rössler oscillators, the transition from the asynchronous to the synchronous regime can reduce the measures of multiscality (Δ_h, Δ_α) as illustrated in Fig. 4b by means of the WTMM-technique. However, it is interesting to note that entrainment in coupled Lorenz systems does not always lead to such an effect. In some situations, variation of the ratio r_2/r_1 shows that synchronization of the oscillations removes the differences between the dynamics of individual

oscillators and decreases the numerical values of the scaling characteristics ($\bar{\alpha}$, $h(0)$) without a clear reduction of the multifractality degree. We conclude that entrainment in the coupled Lorenz model can find varying reflections in the structure of the return time series demonstrating, however, in all cases a simpler dynamics for the synchronous motions.

3.3. Coupled nephrons

Complex oscillations with several different time scales are rather typical for the dynamics of living systems. As an example we have chosen to consider the nephron model [21] that displays relatively fast motions related to the inherent myogenic dynamics of the afferent arterioles combined with slower motions associated with a delay in the so-called tubuloglomerular feedback that controls the diameter of the afferent arteriole in dependence of the ionic composition of the fluid leaving the nephron.

3.3.1. Numerical simulation

The nephron is the functional unit of the kidney. Its main structure is discussed, for instance, in Ref. [21]. The autoregulation of the blood flow to the individual nephron may be described by the following six ordinary differential equations:

$$\begin{aligned} \dot{P}_t &= G(P_t, r), \quad \dot{X}_1 = 3(F_H(P_t) - X_1)/T\,, \\ \dot{r} &= v_r, \qquad \dot{X}_2 = 3(X_1 - X_2)/T\,, \\ \dot{v}_r &= V_{\beta,T}(P_t, r, \beta, X_3), \qquad \dot{X}_3 = 3(X_3 - X_3)/T\,. \end{aligned} \tag{8}$$

The first equation describes the variations of hydrostatic pressure P_t in the proximal tubule in terms of the in- and outgoing fluid flows. The nonlinear function G accounts for the filtration process in the *glomerulus*. The following two equations represent the oscillatory dynamics associated with the arteriolar flow control. Here, r denotes the radius of the active part of the afferent blood vessel, and v is its rate of increase. Note that the right-hand part of the equation for v depends on X_3, reflecting the *tubulo-glomerular feedback* (*TGF*).

The remaining equations in the single-nephron model describe the delay T in the TGF regulation. This delay arises both from the transit time of fluid through the *loop of Henle* and from the cascaded enzymatic processes that are responsible for the adjustment of r. The flow F_H into the loop of Henle is proportional to the difference between P_t and the pressure in the distal tubule. The feedback delay T, that typically assumes a value of 12–18 s, will be considered the main bifurcation parameter in our analysis. Another important parameter is the strength β of the feedback regulation (denoted α in Ref. [21]). This parameter takes a value about 12 for normotensive rats and increases to about 18 for the so-called spontaneously hypertensive rats. For a more detailed explanation of the model equations, control parameters, and the dynamics of nephrons see Ref. [21].

Measurements of the hydrostatic pressure P_t for anesthetized rats show characteristic self-sustained oscillations with a period of 20–40 s [29], and for rats with elevated blood pressure the oscillations tend to become chaotic [30]. Model (8) represents a relatively accurate account of the basic physiological mechanisms responsible for the chaotic dynamics, and over the years it has been tested and examined in many different ways.

Neighboring nephrons can influence each other's blood supply either through vascularly propagated electrical (or electrochemical) signals or through a direct hemodynamic coupling arising via redistribution of the blood flow between the coupled nephrons. In our mathematical model [9,31], the two interaction mechanisms are included via nonlinear functions. Here, we consider pure vascularly propagated coupling with a strength γ. Various forms of synchronous behavior in two interacting nephrons are reported in Ref. [31].

Using the above model we can study the transition to the synchronous chaotic regime for the fast (v_r) and slow (P_t or X_j) components of the dynamics separately. Choosing the secant planes $P_t = 1.6$ kPa and $v_r = 0$ for each of two coupled subsystems we analyze the overall dynamics of the interacting units.

Fig. 6 represents the main results for weak chaos ($\beta = 27.3$, other parameters are the same as in Ref. [31]). Transition to the synchronous state for fast oscillations reduces the degree of multiscality in the return time sequences: Asynchronous dynamics (Fig. 6a, triangles) is obviously characterized by different slopes of the dependence $\lg F$ *vs.* $\lg n$, i.e., by different α-exponents for regions $\lg n < 2.5$ and $\lg n > 2.5$ (therefore, Δ_α is large) whereas the considered dependence becomes closer to a line (Δ_α is reduced) for the synchronous state (Fig. 6a, circles). Here, we clearly see that differences in the structure of the return time series are related to the region of long-range correlations (large values of n). Therefore, these differences may not be quantified by the WTMM-approach (Fig. 6c) which is more appropriate as a tool for the analysis of small scales.

According to the DFA-technique a reduction of both the degree of multiscality and the $\bar{\alpha}$-exponents at the transition to the synchronous behavior take place also for the slow oscillations (Fig. 6b). However, the WTMM-method shows that the degree of multiscality clearly decreases only for positive q related to the large fluctuations in the data series; for negative q such an effect is not observed (Fig. 6d). Note again, that the scaling features for the individual oscillators in the synchronous state are close, unlike the results for asynchronous motions.

Numerical investigations for fully developed chaos ($\beta = 28$) [31] reveal other peculiarities (Fig. 7). Individual units have different scaling properties in the asynchronous regime. For fast motions besides the reduction of the multiscality and the increased probability of anti-correlated behavior, synchronization clearly brings closer the characteristics of the interacting subsystems (Figs. 7a and c). The case of slow motions is more complicated. Following Fig. 7b, the $\bar{\alpha}$-exponents of the DFA-technique decrease for only one subsystem in the synchronous state (slope of the dependence $\lg F$ *vs.* $\lg n$ reduces for black circles in Fig. 7b in comparison with black triangles), for the other subsystem even some increase of $\bar{\alpha}$ may be observed (Fig. 7b, white circles). Obvious differences in the individual dynamics of the interacting units take place inside the

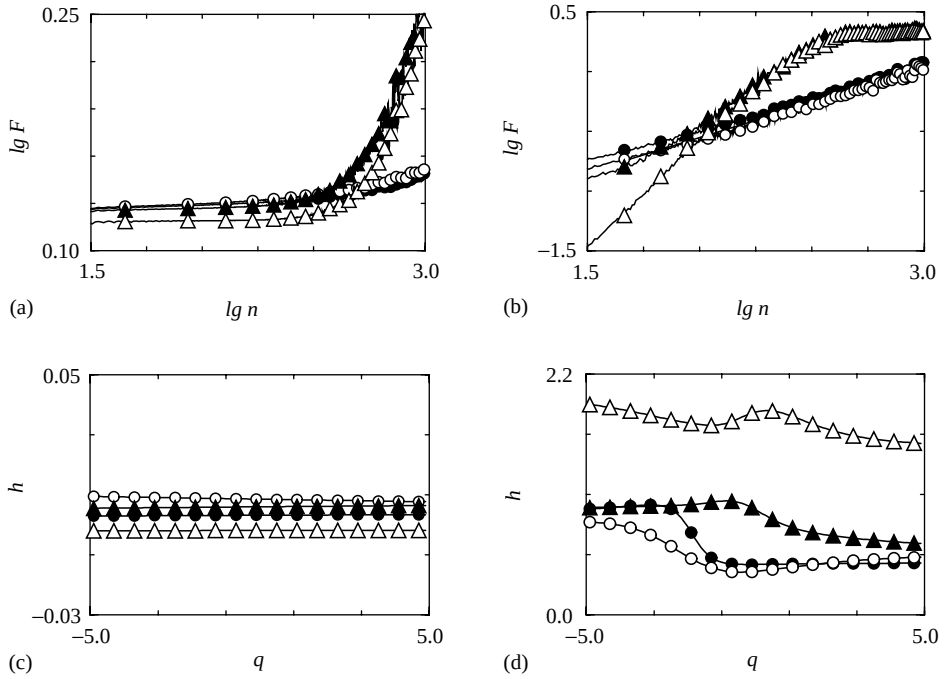

Fig. 6. Scaling properties of the coupled nephron model in the regime of weak chaos ($\beta = 27.3$): $\lg F$ vs. $\lg n$ of the DFA-approach and Hölder exponents of the WTMM-technique for fast (a,c) and slow (b,d) motions. Here, black symbols correspond to the first of the interacting subsystems and white symbols are related to the second subsystem. Circles mark the synchronous dynamics, and triangles label the asynchronous regime.

synchronization region as well as outside this region (Fig. 7d), i.e., unlike the case of the fast phase variables, synchronization does not remove differences between the slow dynamics of the individual units. At the same time, we observe the decreasing multiscality for both subsystems in the synchronous motion. In other words, the transition to the synchronous state for slow oscillations of the chosen regime increases the probability of anti-correlated dynamics of only one of the interacting units and reduces the multiscality degree for both of them. This illustrates specific reflections of the phase synchronization phenomenon in the complex structure of return time series. We can conclude, however, that in all the discussed examples synchronization is accompanied by an obviously simpler structure of the characteristic scales in comparison with the asynchronous motions.

3.3.2. Experimental results

Besides the model describing the dynamics of coupled nephrons we have analyzed experimental data obtained at the Department of Medicine, University of Copenhagen.

Fig. 8 shows an example of the tubular pressure variations that one can observe for adjacent nephrons in a hypertensive rat. These oscillations are quite irregular and

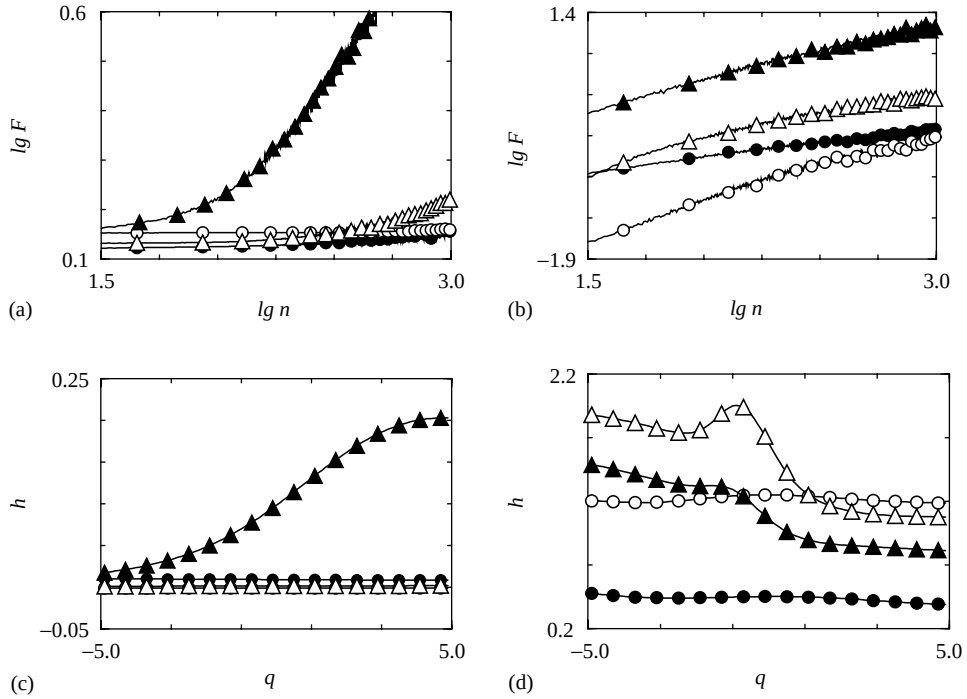

Fig. 7. Scaling properties of the coupled nephron model in the regime of strong chaos ($\beta = 28$): $\lg F$ vs. $\lg n$ of the DFA-approach and Hölder exponents of the WTMM-technique for fast (a), (c) and slow (b), (d) motions. The designations are the same as in Fig. 6.

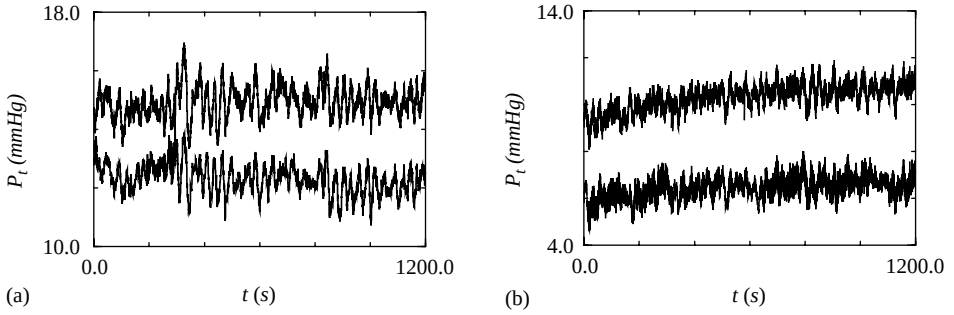

Fig. 8. Experimental data of the proximal tubular pressure for coupled nephrons in a regime of (a) synchronous and (b) asynchronous chaotic dynamics.

a variety of studies have shown that they can be ascribed to a chaotic dynamics. In spite of this complexity, however, one can observe a certain degree of synchronization between the interacting nephrons. Figs. 8a and b illustrate examples of synchronous and asynchronous behavior, respectively. Synchronous dynamics is typically observed

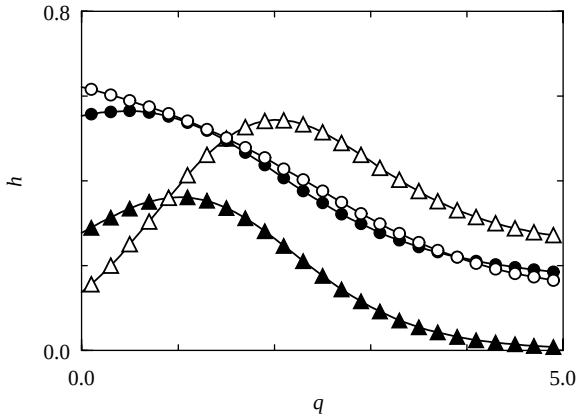

Fig. 9. Hölder exponents of the WTMM-approach estimated from experimental recordings in the synchronous (circles) and the asynchronous (triangles) regimes. Note how the Hölder exponents for the synchronized case are very similar.

for nephrons that share the same interlobular artery, whereas asynchronous dynamics is found for nephrons that derive their blood supply from different blood vessels.

The results of our data analysis are given in Fig. 9. We should note that technical problems connected with the correct extraction of return times from nonstationary data (Fig. 8a) and a relatively short length of the time series (about 10^3 return times) lead to a rather high sensitivity of the Hölder exponents to the choice of secant plane and to the algorithmic parameters (especially for $q < 0$). That is why, in Fig. 9, we present the dependences $h(q)$ only for $q > 0$. Here, the scaling properties of the two interacting units are quite close in the case of synchronous dynamics (Fig. 9, circles), and they do not coincide for the asynchronous regime (Fig. 9, triangles). However, reduction of the degree of multiscality does not occur.

4. Conclusions

During the last few years, multifractality (or, more generally, multiscality) in the evolutionary dynamics of complex systems has become a topic of significant interest in many areas of science. In this paper, we studied the possibility of a multifractal characterization of the synchronization phenomenon in two coupled chaotic oscillators. Taking three models with different dynamics, namely, coupled Rössler oscillators, coupled Lorenz systems, and coupled nephrons, we analyzed how the transitions between different types of synchronous and asynchronous motions is reflected in the structure of characteristic temporal scales represented, for instance, via return times to a Poincaré section. The main results are:

Chaotic phase synchronization in the coupled Rössler systems is accompanied by significant changes of the return time series including (i) a reduction in the degree of multiscality or even a loss of multifractality; (ii) a decrease of “smoothness” for the

return time sequence that can be quantified by a reduction of the $\bar{\alpha}$-exponents (here, a transition from correlated behavior for the asynchronous motions to anti-correlations for the synchronous regime takes place); (iii) a removal of differences between the individual dynamics of the interacting units.

Entrainment in systems with several time-scales (Lorenz or nephron models) is more complicated. In particular, the scaling features may be different for different phase variables and the reflection of the synchronization phenomenon in the temporal scales can vary. We may note that the three effects observed for coupled Rössler oscillators can also occur in the presence of several characteristic scales in the motions of the interacting subsystems. However, we typically observe different combinations of these effects. Sometimes, they can all be seen simultaneously. In other cases, chaotic phase synchronization decreases the "smoothness" of the return time series and removes differences between the individual dynamics of the coupled oscillators without a clear reduction of the measures of multiscality. Finally, the degree of multiscality can decrease significantly while the actual regimes of the interacting units remain different. We can conclude that the synchronization in systems of coupled chaotic oscillators with several temporal scales can have different reflections, with the return time dynamics involving a combination of some general effects.

Application of the above methods to experimental data allow us to diagnose the synchronous and asynchronous behavior of complex oscillations. This was illustrated by means of experimental results for coupled functional units in the kidney.

Acknowledgements

This work was supported by the Danish Natural Science Foundation and INTAS 01-2061. A.P. and A.Z. acknowledge the support of CRDF (Award REC-006). O.S. acknowledges INTAS (Grant YSF 01/1-0023).

References

[1] V.I. Arnol'd, Am. Math. Soc. Transl., Ser. 2 46 (1965) 213–284.
[2] A. Pikovsky, M. Rosenblum, J. Kurths, Synchronization: A Universal Concept in Nonlinear Sciences, Cambridge Nonlinear Science Series 12, Cambridge University Press, Cambridge, 2001.
[3] L.M. Pecora, T.L. Carroll, Phys. Rev. Lett. 64 (1990) 821.
[4] H. Fujisaka, Y. Yamada, Progr. Theor. Phys. 69 (1983) 32;
V.S. Afraimovich, N.N. Verichev, M.I. Rabinovich, Radiophys. Quantum Electron. 29 (1986) 795.
[5] M.G. Rosenblum, A.S. Pikovsky, J. Kurths, Phys. Rev. Lett. 78 (1997) 4193.
[6] N.F. Rulkov, M.M. Sushchik, L.S. Tsimring, H.D.I. Abarbanel, Phys. Rev. E 51 (1995) 980;
L. Kocarev, U. Parlitz, Phys. Rev. Lett. 76 (1996) 1816.
[7] M.G. Rosenblum, A.S. Pikovsky, J. Kurths, Phys. Rev. Lett. 76 (1996) 1804.
[8] L. Kocarev, U. Parlitz, Phys. Rev. Lett. 74 (1995) 5028.
[9] E. Mosekilde, Yu. Maistrenko, D. Postnov, Chaotic Synchronization: Applications to Living Systems, World Scientific, Singapore, 2002.
[10] V.S. Anishchenko, T.E. Vadivasova, D.E. Postnov, M.A. Safonova, Int. J. Bifurcation Chaos 2 (1992) 633.
[11] T.E. Vadivasova, A.G. Balanov, O.V. Sosnovtseva, D.E. Postnov, E. Mosekilde, Phys. Lett. A 253 (1999) 66.

[12] A. Neiman, A. Silchenko, V. Anishchenko, L. Schimansky-Geier, Phys. Rev. E 58 (1998) 7118–7125.
[13] B.B. Mandelbrot, Fractals and Multifractals: Noise, Turbulence and Galaxies, Selecta Vol. 1, Springer, New York, 1989;
A. Bunde, S. Havlin (Eds.), Fractals in Science, Springer, Berlin, 1994.
[14] T.C. Halsey, M.H. Jensen, L.P. Kadanoff, I. Procaccia, B.I. Shraiman, Phys. Rev. A 33 (1986) 1141;
T. Tel, Z. Naturforsh. 43a (1988) 1154;
M.H. Jensen, G. Paladin, A. Vulpiani, Phys. Rev. Lett. 67 (1991) 208.
[15] P.Ch. Ivanov, L.A.N. Amaral, A.L. Goldberger, S. Havlin, M.G. Rosenblum, Z.R. Struzik, H.E. Stanley, Nature 399 (1999) 461.
[16] R. Benzi, L. Biferale, G. Paladin, A. Vulpiani, M. Vergassola, Phys. Rev. Lett. 67 (1991) 2299;
E. Mosekilde, J.S. Thomsen, C. Knudsen, R. Feldberg, Physica D 66 (1993) 143;
C.L. Berthelsen, J.A. Glazier, S. Raghavachari, Phys. Rev. E 49 (1994) 1860;
J. Arrault, A. Arneodo, A. Davis, A. Marshak, Phys. Rev. Lett. 79 (1997) 75;
A. Silchenko, C.-K. Hu, Phys. Rev. E 63 (2001) 041105.
[17] S.V. Buldyrev, A.L. Goldberger, S. Havlin, C.-K. Peng, M. Simons, H.E. Stanley, Phys. Rev. E 47 (1993) 4514;
C.-K. Peng, S. Havlin, H.E. Stanley, A.L. Goldberger, Chaos 5 (1995) 82.
[18] J.F. Muzy, E. Bacry, A. Arneodo, Phys. Rev. Lett. 67 (1991) 3515.
[19] J.F. Muzy, E. Bacry, A. Arneodo, Int. J. Bifurcation Chaos 4 (1994) 245.
[20] C. Nicolis, G. Nicolis, Phys. Rev. A 34 (1986) 2384.
[21] E. Mosekilde, Topics in Nonlinear Dynamics. Applications to Physics, Biology and Economic Systems, World Scientific, Singapore, 1996.;
M. Barfred, E. Mosekilde, N.-H. Holstein-Rathlou, Chaos 6 (1996) 280.
[22] S.V. Buldyrev, A.L. Goldberger, S. Havlin, R.N. Mantegna, M.E. Matsa, C.-K. Peng, M. Simons, H.E. Stanley, Phys. Rev. E 51 (1995) 5084;
S. Havlin, S.V. Buldyrev, A. Bunde, A.L. Goldberger, P.Ch. Ivanov, C.-K. Peng, H.E. Stanley, Physica A 273 (1999) 46.
[23] C.-K. Peng, S.V. Buldyrev, A.L. Goldberger, S. Havlin, M. Simons, H.E. Stanley, Phys. Rev. E 47 (1993) 3730.
[24] U. Frish, G. Parisi, in: M. Ghil, R. Benzi, G. Parisi (Eds.), Turbulence and Predictability in Geophysical Fluid Dynamics and Climate Dynamics, North-Holland, Amsterdam, 1985, p. 71.
[25] D.E. Postnov, T.E. Vadivasova, O.V. Sosnovtseva, A.G. Balanov, V.S. Anishchenko, E. Mosekilde, Chaos 9 (1999) 227;
T.E. Vadivasova, O.V. Sosnovtseva, A.G. Balanov, V.V. Astakhov, Discrete Dynamics in Nature and Science 4 (2000) 231.
[26] A.N. Pavlov, O.V. Sosnovtseva, E. Mosekilde, Phys. Rev. E (2002), submitted.
[27] V.S. Anishchenko, A.N. Silchenko, I.A. Khovanov, Phys. Rev. E 57 (1998) 316.
[28] S. Mallat, W.L. Hwang, IEEE Trans. Inf. Theory 38 (1992) 617.
[29] P.P. Leyssac, L. Baumbach, Acta Physiol. Scand. 117 (1993) 415.
[30] K.-P. Yip, N.-H. Holstein-Rathlou, D.J. Marsh, Am. J. Physiol. 261 (1991) F400.
[31] D.E. Postnov, O.V. Sosnovtseva, E. Mosekilde, N.-H. Holstein-Rathlou, Int. J. Mod. Phys. B 15 (2001) 3079.